Geophys. J. Int. (2022) **23X**, **??–??**

Investigation of dipolar dominancy in geodynamo simulations with different inner core sizes

Y. Nishida[1], Y. Katoh[1], H. Matsui[2], M. Matsushima[3], T. Kera[1], and A. Kumamoto[1]

[1] *Department of Geophysics, Tohoku University, Sendai, Japan*
[2] *Department of Earth and Planetary Sciences, University of California Davis, Davis, California, USA*
[3] *Department of Earth and Planetary Sciences, Tokyo Institute of Technology, Tokyo, Japan*

SUMMARY

The solid inner core of the Earth has been growing for approximately one billion years due to cooling of the Earth. The changing spherical shell geometry of the Earth's core is likely to influence on the geodynamo driven by convective motions in the fluid outer core. To understand the geometry effect on the dynamo regime through evolution of the core, we perform numerical simulations of geodynamo with three spherical shell radius ratios: $r_i/r_o = 0.15$, 0.25, and 0.35, where r_i and r_o are the inner and outer core radii, respectively. To evaluate the morphology of the magnetic field, we examine two indices about dipole component dominance: (i) f_{dip}, dipolarity used to assess the relative strength of the dipole field at the core surface in numerical dynamo models; and (ii) f_{mag_fit}, the ratio of magnetic energy density for the dipole component to that extrapolated from the magnetic power spectrum for the high degree components. We investigate the field morphology estimated from f_{dip}, and f_{mag_fit}, and find that f_{mag_fit} is valid to determine the dynamo regime, even if f_{dip} suggests a transition regime between dipolar and non-dipolar dominance. We also investigate the range of Rayleigh number for sustained dynamos based on f_{dip} and f_{mag_fit}, and find that the range of Rayleigh number for a dynamo characterized by a strong dipole field becomes narrower for a smaller inner core. The f_{dip}–dependence on the Rayleigh number for $r_i/r_o = 0.25$ and 0.35 is similar each other, whereas the f_{mag_fit}–dependence for $r_i/r_o = 0.35$ is found to be relatively larger than that for $r_i/r_o = 0.25$. On the other hand, small values of f_{dip} and f_{mag_fit} for $r_i/r_o = 0.15$ suggest that the dynamo regime is characterized not by a strong dipole field but by non-dipolar dominance. These results indicate that changes in the spherical shell radius ratio largely influence on the dynamo regime in numerical dynamos with a fixed temperature boundary condition.

Key words: Dynamo; Theories and simulations; Magnetic field variations through time; Numerical solutions

1 INTRODUCTION

The Earth has an intrinsic magnetic field. The dynamo action of liquid iron alloy convection in the outer core generates the geomagnetic field. The fluid alloy gains buoyancy from the cooling of the Earth. Upon cooling, the inner core nucleated as liquid iron solidified from the center of the fluid core at high pressure. Compositional convection, which is associated with the growth of the inner core, is also a source of outer core convection. Recent thermochemical calculations suggest that the inner core which formed approximately one billion years ago and the inner core has been continually growing to its present size (Labrosse *et al.* 2001). Although the size of the inner core has been changing across the geological time scale, the intensity of the geomagnetic field described by the virtual dipole moment (VDM) has maintained its present intensity for more than 3.5 billion years based on paleomagnetic observations (Biggin *et al.* 2015); the geodynamo has been sustained during this period.

Previous studies have performed a number of numerical dynamo simulations under the assumption of the present geometry of the Earth's core; the aspect ratio of the inner core radius, r_i, to the outer core radius, r_o, is $r_i/r_o = 0.35$. For example, Christensen *et al.* (Christensen & Aubert, 2006) revealed, in detail, sustained dynamo conditions for various control parameters. They clarified dipolar dynamo cases and non-dipolar dynamo cases. The dynamo regime changes from stable dipolar to reversing non-dipolar with increase of the Rayleigh numbers (Kutzner and Christensen, 2002; Olson *et al.* 2011).

In the smaller inner core setting, as compared with the present size, however, there have been a few attempts at a numerical dynamo. Some numerical dynamo studies have shown that the geometry effect on the dynamo regime is small. Hori *et al.* (Hori *et al.* 2010) investigated the morphology of a magnetic field with fixed temperature (FT) and fixed heat flux (FF) boundary conditions for two spherical shell radius ratios: $r_i/r_o = 0.10$ and 0.35. Regardless of the difference in radius ratios, they found that sus-

tained dynamos were dipolar under the FF boundary condition and non-dipolar under the FT boundary condition. Driscoll (2016) carried out numerical simulations of geodynamo for eleven patterns of radius ratios in the range of $0.10 < r_i/r_o < 0.35$ and core power derived from a thermal evolution model. Driscoll (2016) found that the total magnetic energy in a spherical shell increased with increase of the ratios r_i/r_o and that sustained dynamos were characterized by a strong dipole magnetic field.

Other numerical dynamo studies have shown that the inner core size influences dipolar dominance. Heimpel *et al.* (2005) investigated dynamo onset conditions for six spherical shell radius ratios: $0.15 < r_i/r_o < 0.65$. They found that the dipolar and total magnetic energy at the core–mantle boundary (CMB) decreases with decrease of r_i/r_o values for $r_i/r_o < 0.45$. Lhuillier *et al.* (2019) also reported on the effect of geometry on the dynamo regime. They performed chemically driven geodynamo simulations by changing ten patterns of radius ratios in the range of $0.10 < r_i/r_o < 0.44$. They found that sustained magnetic fields were dipolar for $r_i/r_o < 0.18$ and $r_i/r_o > 0.26$, whereas they were less dipolar for $0.20 < r_i/r_o < 0.22$. Although some studies have attempted to reveal the dependence of the dynamo regime on the spherical shell radius ratio, we do not yet fully understand how the morphology of the magnetic field is determined.

In recent numerical dynamos, dipolarity, $f_{\rm dip}$, which is defined as the ratio of the dipole field strength to the total field strength at the CMB (Christensen & Aubert, 2006), has been widely used as an index for assessing the morphology of geomagnetic field. Christensen & Aubert (2006) mention that the magnetic field is dipolar-dominated when f_{dip} exceeds 0.35. This criterion for the dynamo regime is valid when dynamos are categorized into large and small f_{dip} groups (Soderlund *et al.* 2012). However, this criterion is not valid when dynamos are not categorized by dipolarity (Aubert *et al.* 2009).

The observed dipolar-dominated geomagnetic field can be expressed in terms of the magnetic power spectrum at the Earth's surface (Lowes 1974) and at the CMB (Langel & Estes 1982). While Kono & Roberts (2002) compared a power spectrum of the observed geomagnetic field with that of numerical dynamos, there was a lack of quantitative evaluation of the dipolar dominance. As the dipolarity has no information of magnetic power spectrum distribution in higher degrees, we require not only the dipolarity, but also another index that represents dipolar dominance assessed from the spectrum distribution.

Although numerical dynamo simulations are useful tools to investigate magnetic field intensity and structure in the past Earth environment, previous studies have not yet established the criterion to evaluate dipolar dominance. The purpose of this study is to investigate the dynamo conditions of a sustained dipolar or non-dipolar dynamo for some spherical shell radius ratios based on an evaluation of dipolar dominance. Hence, we carried out numerical simulations of geodynamo for three spherical shell radius ratios, i.e., $r_i/r_o = 0.15$, 0.25, and 0.35. To focus on how convection occurs, the Rayleigh number (Ra) was only treated as a variable. The Ra is a parameter related to buoyancy, which is the driving force of convection. By simulating a wider range in the Ra than previous studies, we can compare cases of a small inner core size setting with those of the present size. A combination of the dipolarity at the CMB, as well as the magnetic energy spectrum at the CMB in the spherical harmonic degree expansion, reveal the range in the Ra in the sustained dipolar or non-dipolar dynamo for each radius ratio.

2 METHOD

A numerical geodynamo model is given by an electrically conducting Boussinesq fluid in a rotating spherical shell. The governing equations of the geodynamo in the outer core are described by the momentum equation, heat equation, continuity equation, magnetic induction equation, and Gauss's law for the magnetic field, which are respectively given as

$$\begin{aligned}\frac{\partial \boldsymbol{u}}{\partial t} + (\boldsymbol{\omega}\times\boldsymbol{u}) &= -\nabla\left(P+\frac{1}{2}u^2\right) - \nabla\times\nabla\times\boldsymbol{u} - \frac{2}{E}(\hat{z}\times\boldsymbol{u}) \\ &\quad + \frac{Ra}{Pr}T\frac{\boldsymbol{r}}{r_o} + \frac{1}{PmE}(\boldsymbol{J}\times\boldsymbol{B}), \qquad (1)\\ \nabla\cdot\boldsymbol{u} &= 0, \qquad (2)\\ \frac{\partial T}{\partial t} + (\boldsymbol{u}\cdot\nabla)T &= \frac{1}{Pr}\nabla^2 T, \qquad (3)\\ \frac{\partial \boldsymbol{B}}{\partial t} &= -\frac{1}{Pm}\nabla\times\nabla\times\boldsymbol{B} + \nabla\times(\boldsymbol{u}\times\boldsymbol{B}), \qquad (4)\end{aligned}$$

and

$$\nabla\cdot\boldsymbol{B} = 0, \qquad (5)$$

where $\boldsymbol{u}$, P, T, $\boldsymbol{B}$, and $\hat{z}$ are the velocity, pressure, temperature, magnetic field, and unit vector along the rotation axis, respectively. $\boldsymbol{\omega} = \nabla\times\boldsymbol{u}$ and $\boldsymbol{J} = \nabla\times\boldsymbol{B}$ are the vorticity and current density, respectively. In Eqs. (1)–(5), the length and temperature are normalized by the outer core thickness, $L = r_o - r_i$ and average temperature difference between the inner core boundary (ICB) and the CMB, ΔT, respectively. The time is normalized by the kinematic viscosity diffusion time, $\tau_\nu = L^2/\nu$, where ν is the kinetic viscosity, and the magnetic field is normalized by $\sqrt{\rho_0\mu_0\eta\Omega}$, where ρ_0, μ_0, η, and Ω are the average density, magnetic permiability, magnetic diffusivity, and angular velocity of system's rotation, respectively. The Rayleigh number, Ra, Ekman number, E, Prandtl number, Pr, and magnetic Prandtl number, Pm are defined as follows:

$$Ra = \frac{\alpha g_o \Delta T L^3}{\kappa\nu}, E = \frac{\nu}{\Omega L^2}, Pr = \frac{\nu}{\kappa}, \text{ and } Pm = \frac{\nu}{\eta}, \qquad (6)$$

where, α, g_o, and κ are the thermal expansion, gravity at the outer boundary of the shell, and thermal diffusivity, respectively.

We used the numerical dynamo code Calypso (Matsui *et al.* 2014). In Calypso, the spherical harmonic expansion method is used in the horizontal discretization, and the second-order finite differences are used in the radial discretization. For the time integrations, the Crank-Nicolson method was used in the linear diffusive terms and the second order Adams-Bashforth method was used in the other terms.

At the initial condition, temperature perturbation was applied to all the sectorial modes. The initial magnetic field was set as an axial dipole based on Christensen *et al.* (2001). For the boundary condition, the temperatures at the CMB and ICB were fixed as $T(r_o) = 0$ and $T(r_i) = 1$, respectively. The mantle and inner core were assumed to be co-rotating, and a non-slip boundary ($\boldsymbol{u} = 0$) was applied to the CMB and ICB. The mantle and inner core were assumed to be electrically insulated, and the magnetic field at the boundaries was connected to the potential field. In the parameter setting, Ra was changed among the cases; the Ekman, Prandtl, and magnetic Prandtl numbers were fixed at $E = 10^{-3}$, $Pr = 1$, and $Pm = 5$ in all simulation cases. The truncation of the spherical harmonics and the radial grid points were set to $L_{max} = 47$ and $N_r = 63$, respectively. To eliminate aliasing in the spherical harmonic expansion, horizontal grids were set to $(N_\theta, N_\phi) = (72, 144)$. To investigate the effects of different inner

core sizes, the spherical shell radius ratios of the inner core radius to the outer core radius were set as $r_i/r_i = 0.15$, 0.25, and 0.35. First, we performed numerical simulations of non-magnetic thermal convection in rotating spherical shells to estimate the critical Rayleigh number, Ra_{crit}, for the onset of thermal convection. We then carried out numerical simulations of magnetohydrodynamic (MHD) dynamos driven by thermal convection. Dynamo simulations with a lower Ekman number are necessary, however, we were forced to perform dynamo simulations with $E = 10^{-3}$ to investigate various Rayleigh numbers and inner core radii for computational limitation like dynamo simulations of Lhuillier *et al.* (2019), in which the Ekman number is larger than $E = 10^{-3}$.

3 RESULTS

3.1 Estimation of the critical Rayleigh number

To estimate the critical Rayleigh number ($Ra_{\rm crit}$), equations (1)–(3) without the Lorentz force term $(PmE)^{-1}(\boldsymbol{J}\times\boldsymbol{B})$, were solved as non-magnetic thermal convection simulations. The kinetic energy density was calculated for the average of $t/\tau_\nu = 4.5$ to 6 in viscous diffusion time as follows:

$$E_{\rm kin} = \frac{1}{V_S}\int_{V_S}\frac{1}{2}\boldsymbol{u}^2 dV, \tag{7}$$

where V_S is the volume of the spherical shell.

$E_{\rm kin}$ listed in Table 1 is calculated as a mean over a quasi-steady state, and is found to be linearly related to, as shown in Fig. 1. The critical Rayleigh numbers are estimated as $Ra_{\rm crit} = 1.09\times10^5$, 0.72×10^5, and 0.56×10^5 in $r_i/r_o = 0.15$, 0.25, and 0.35, respectively, by the same method as Al-Shamali *et al.* (2004). The obtained values of $Ra_{\rm crit}$ were almost identical to those reported in Al-Shamali *et al.* (2004) for the same parameters and conditions used in this study. $Ra_{\rm crit}$ is large when the aspect ratio is smaller, indicating that convection in a rotating, thick spherical shell requires a large buoyancy.

3.2 MHD simulation results

We performed MHD dynamo simulations for various Rayleigh numbers and the radius ratios using Eqs (1)–(5). The magnetic energy density was calculated as follows:

$$E_{mag} = \frac{1}{V_S EPm}\int_{V_S}\frac{1}{2}\boldsymbol{B}^2 dV. \tag{8}$$

Tables 3.2, 3.2, and 4 list results of MHD dynamo simulations. We performed respective numerical simulations for at least two magnetic diffusion times to assess whether the magnetic field was sustained or dissipated. For example, Fig. 2 shows the time evolution of the kinetic and magnetic energy density at $Ra/Ra_{\rm crit} = 2.8$ for $r_i/r_o = 0.25$. In this case, the magnetic field was sustained. We calculated the time average of the kinetic and magnetic energy density, as well as the dipolarity over a 0.5 magnetic diffusion time, at the end of each case (see shaded area in Fig. 2). The kinetic and magnetic energy density as a function of Rayleigh number is shown in Fig. 3. In each radius ratio case with a sustained magnetic field, the $E_{\rm kin}$ values in the MHD cases were smaller than the $E_{\rm kin}$ values in the corresponding non-MHD cases. These results show that the Lorentz force caused by the intense magnetic field disturbs convection. There were differences among the three radius ratio cases. At $r_i/r_o = 0.15$, the $E_{\rm mag}$ values in the MHD cases were smaller than the $E_{\rm kin}$ values in the MHD cases for all cases. This trend is consistent with the results of Heimpel *et al.* (2005), whose simulations were performed around dynamo onset. At $r_i/r_o = 0.25$, the values of $E_{\rm mag}$ in the MHD cases were either smaller or larger than the $E_{\rm kin}$ values in the MHD. For cases of $Ra/Ra_{\rm crit} = 3.6$ and 4.0, the $E_{\rm mag}$ values were significantly smaller than those for the cases of other Rayleigh numbers. Although the trend in the magnetic energy spectrum did not change, there was a decrease in the amplitude. At $r_i/r_o = 0.35$, the values of $E_{\rm mag}$ in the MHD cases were larger than the values of $E_{\rm kin}$ in the MHD cases for almost all cases. From the above, it is not likely to sustain a strong magnetic field with a smaller inner core.

Fig. 4 shows the radial component of the magnetic field at the CMB and the equatorial cross-sections of the z-component of the vorticity and magnetic field are plotted at $Ra/Ra_{\rm crit} = 11.9$ for $r_i/r_o = 0.15$. The same plots at $Ra/Ra_{\rm crit} = 3.1$ for $r_i/r_o = 0.25$ and at $Ra/Ra_{\rm crit} = 3.0$ for $r_i/r_o = 0.35$ are shown in Figs 5 and 6, respectively. At the equatorial plane, the magnetic field is concentrated in the anti-cyclone columns to generate a dipolar field at $r_i/r_o = 0.25$ and 0.35; intense magnetic patches are located near the tangent cylinder, which is an imaginary cylinder tangent to the inner-core equator and coaxial with the rotation axis. In the case of $r_i/r_o = 0.15$ case, strong convection is generated locally, where strong B_Z convection is generated between the cyclonic and anti-cyclonic columns at the equatorial plane. As these intense magnetic fields are not concentrated in the convection columns, the radial magnetic field at the CMB near the tangent cylinder has a quadrupolar (symmetric with respect to the equator) and is smaller than that of the cases with different aspect ratios.

Table 1. Average kinetic energy density E_{kin} at the quasi-steady state for the thermal convection without the magnetic field

$r_{\rm i}/r_{\rm o}$	$Ra[\times10^5]$	$E_{\rm kin}$
0.15	1.0	8.31×10^{-6}
0.15	1.2	5.72
0.15	1.25	8.15
0.15	1.3	10.62
0.15	1.35	13.16
0.15	1.4	15.80
0.15	1.45	18.54
0.25	0.70	8.55×10^{-4}
0.25	0.75	2.41
0.25	0.78	4.94
0.25	0.80	6.62
0.25	0.82	8.35
0.25	0.85	11.02
0.25	0.90	15.70
0.35	0.55	1.76×10^{-4}
0.35	0.58	2.38
0.35	0.60	4.54
0.35	0.62	6.76
0.35	0.65	10.22
0.35	0.67	12.60
0.35	0.70	16.28

Table 2. Time average of the kinetic energy $E_{\rm kin}$, magnetic energy $E_{\rm mag}$, dipolarity $f_{\rm dip}$, and Elsasser number Λ for the cases with $r_{\rm i}/r_{\rm o} = 0.15$

$Ra[\times 10^3]$	$Ra/Ra_{\rm crit}$	$E_{\rm kin}$	$E_{\rm mag}$	$f_{\rm dip}$	$f_{\rm mag\_fit}$	$\Lambda_{\rm d}$
760	7.0	823.7	5.193	–	–	–
870	8.0	801.4	501.6	0.494	1.435	0.105
980	9.0	846.37	579.0	0.516	1.866	0.116
1100	10.1	748.36	444.7	0.349	0.860	0.053
1300	11.9	1493	300.5	0.117	0.322	0.068
1500	13.8	1867	135.6	0.155	0.391	0.034
1700	15.6	2141	234.3	0.172	0.420	0.054

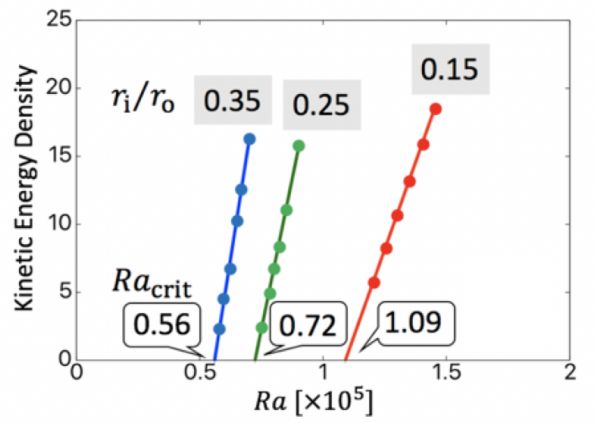

Figure 1. The kinetic energy density, as a function of the Rayleigh number, calculated in spherical shells with different geometries. Red, green, and blue lines indicate the linear fitting for $r_i/r_o = 0.15$, 0.25, and 0.35, respectively.

4 DISCUSSION

In numerical dynamos, dipolarity is used for quantification of the magnetic field morphology at the CMB. Although dipolarity has been evaluated in some numerical dynamos (Christensen & Aubert, 2006; Soderlund *et al.* 2012), it is not sufficiently valid in dynamos whose dipolarities are gradually changing (e.g., Aubert *et al.* 2009). In an observational magnetic field, the dipole is assessed by how far the dipolar component is from the trend of higher degree components (Lowes 1974; Langel & Estes 1982). We quantitatively evaluated dipolar component dominance in combination with the dipolarity, comparison of the dipolar magnetic energy, and an extrapolation of $l = 1$ based on the fitting curve of higher degrees.

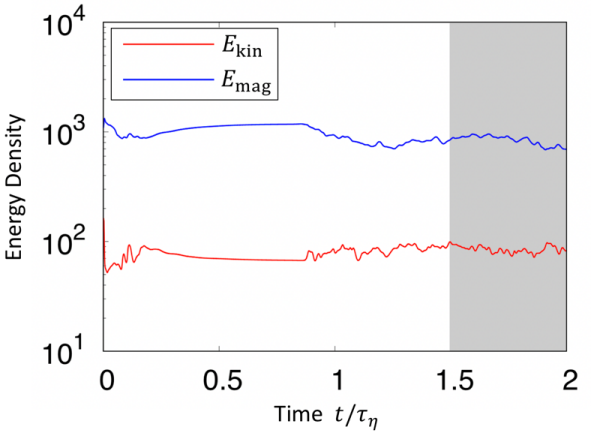

Figure 2. Time evolution of the kinetic and magnetic energy densities in the case of sustained dynamo at $Ra/Ra_{\rm crit} = 2.8$ with $r_i/r_o = 0.25$. The red and blue lines mean the kinetic and magnetic energy density, respectively.

To quantitatively evaluate the axial dipole component dominancy, we calculated the dipolarity at the CMB, which is defined as follows:

$$f_{\rm dip} = \left(\frac{E_{mag}^{(l=1,m=0)}(r=r_o)}{\sum_{l=1}^{l_{\rm max}} \sum_{m=0}^{l} E_{\rm mag}^{l,m}(r=r_o)} \right)^{1/2}, \quad (9)$$

where the magnetic energy at the CMB, $E_{\rm mag}(r = r_o)$, is calculated as follows:

$$E_{\rm mag}(r=r_o) = \frac{1}{V_s EPm} \int_S \frac{1}{2} \boldsymbol{B}^2 dS. \quad (10)$$

Fig. 7 shows the dipolarity as a function of the Rayleigh number for $r_i/r_o = 0.15$, 0.25, and 0.35. The dipolarity gradually decreases with an increasing Rayleigh number for $r_i/r_o = 0.25$ and 0.35. The axial dipolar component becomes weak during intense convection. The dependency of the dipolarity on the Rayleigh number is similar for the two radius ratio cases, i.e., $r_i/r_o = 0.25$ and 0.35. Here, $f_{\rm dip}$ is always larger than 0.35 at $r_i/r_o = 0.25$ and 0.35. In contrast, this tendency is different at $r_i/r_o = 0.15$. Furthermore, $f_{\rm dip}$ is larger than 0.45 at $Ra/Ra_{\rm crit} = 8.0$ and 9.0 while f_{dip} is smaller than 0.35 at $Ra/Ra_{\rm crit} > 10.1$.

The results of a number of previous numerical dynamo simulations determine the threshold of the dipolar dominance for $f_{\rm dip} = 0.35$. To obtain a clearer threshold for the dipole dominance, we focused on the magnetic energy spectrum at the CMB as a function of the spherical harmonic degree, l. For example, Fig. 8 shows the magnetic energy density as a function of the spherical harmonic degree at $Ra/Ra_{\rm crit} = 2.8$ for $r_i/r_o = 0.25$. Using odd-degree components in the magnetic energy from $l = 3$ to 19, we evaluated the fitting curve as 46.21×1.481^{-l}. At degree $l = 1$, the $E_{\rm mag}$ of the simulation data $E^{l=1}_{\rm mag\_data}$ was compared with that from the extrapolated value in the fitting function $E^{l=1}_{\rm mag\_fitting}$. Then, we acquired the ratio of $E_{\rm mag}$ for the simulation result to that from the extrapolated value, $E^{l=1}_{\rm mag\_data}/E^{l=1}_{\rm mag\_fitting}$ (hereafter referred to as $f_{\rm mag\_fit}$. We can assess the dipolar component dominance from a higher degree trend based on how much the ratio of the extrapolation from fitting f_{mag_fit} is larger than 1. Here, $f_{\rm mag\_fit}$ was calculated in all cases and plotted as a function of the Rayleigh number at $r_i/r_o = 0.15$, 0.25, and 0.35 (Fig. 9). At $r_i/r_o = 0.15$, $f_{\rm mag\_fit}$ was smaller than 1 at $Ra/Ra_{\rm crit} > 10.1$. At $r_i/r_o = 0.25$, $f_{\rm mag\_fit}$ was approximately 2.1 at $Ra/Ra_{\rm crit} = 2.2$ and gradu-

Table 3. Time average of the kinetic energy $E_{\rm kin}$, magnetic energy $E_{\rm mag}$, dipolarity $f_{\rm dip}$, and Elsasser number Λ for the cases with $r_{\rm i}/r_{\rm o} = 0.25$

$Ra[\times 10^3]$	$Ra/Ra_{\rm crit}$	$E_{\rm kin}$	$E_{\rm mag}$	$f_{\rm dip}$	$f_{\rm mag\_fit}$	$\Lambda_{\rm d}$
140	1.9	76.69	1.491×10^{-4}	–	–	–
160	2.2	59.05	958.6	0.860	2.116	0.355
180	2.5	62.89	1097	0.867	2.397	0.410
200	2.8	85.49	844.4	0.784	1.828	0.323
220	3.1	103.9	769.2	0.757	2.441	0.283
260	3.6	236.4	48.4	0.644	2.477	0.021
290	4.0	289.3	83.0	0.620	2.610	0.035
330	4.6	248.6	753.8	0.602	2.287	0.277
360	5.0	297.7	769.0	0.562	1.935	0.224
430	6.0	455.6	491.0	0.522	1.887	0.174
500	6.9	642.2	305.2	0.456	1.551	0.130
580	8.1	906.8	126.0	0.412	1.556	0.059
700	9.7	1221	25.4	–	–	–

ally decreased to 1.6 with increase of $Ra/Ra_{\rm crit}$ of up to approximately 8.0. At $r_i/r_o = 0.35$, $f_{\rm mag\_fit}$ was approximately 4.7 at $Ra/Ra_{\rm crit} = 2.0$, gradually decreasing to 2.1 with increase of $Ra/Ra_{\rm crit}$ of up to approximately 7.0.

Comparing the result between f_{dip} and $f_{\rm mag\_fit}$, the common point is that the dipolar dominance decreases with an increasing Rayleigh number. At $r_i/r_o = 0.15$, the dipolar non-dominance can be represented by $Ra/Ra_{\rm crit} > 10.1$ for both indices. At $r_i/r_o = 0.25$ and 0.35, the magnitude relationship of $f_{\rm dip}$ and $f_{\rm mag\_fit}$ is reversed at a small $Ra/Ra_{\rm crit}$ value. Because the magnetic energy of higher degrees is relatively larger for the total energy at $r_i/r_o = 0.35$ than at $r_i/r_o = 0.25$, $f_{\rm dip}$ is smaller at $r_i/r_o = 0.35$ than at $r_i/r_o = 0.25$. Although $E^{l=1}_{\rm mag\_fitting}$ is almost the same at $r_i/r_o = 0.25$ and 0.35, $E^{l=1}_{\rm mag\_data}$ is significantly larger, such that $f_{\rm mag\_fit}$ is larger at $r_i/r_o = 0.35$ than at $r_i/r_o = 0.25$. The difference between $f_{\rm dip}$ and $f_{\rm mag\_fit}$ derives from whether a higher-degree spectrum is taken into account or not. The dependency of the dipolar dominance on the radius ratio can be revealed by $f_{\rm mag\_fit}$ as it contains information from a higher degree spectrum.

We show an example in which we could not categorize the dipole or non-dipole based only on the dipolarity, i.e., the cases for $f_{\rm dip} = 0.376$ at $Ra/Ra_{\rm crit} = 7.1$ with $r_i/r_o = 0.35$ and $f_{\rm dip} = 0.349$ at $Ra/Ra_{\rm crit} = 10.1$ for $r_i/r_o = 0.15$. Fig. 10 shows the CMB spectra for these two cases. The dipolar component is dominant against the high degree trend in the former case while it is not dominant in the latter case. The ratio of extrapolation from the fitting is $f_{\rm mag\_fit} = 2.071$ in the former case and $f_{\rm mag\_fit} = 0.860$ in the latter case; we observed that the former case is dipolar-dominated while the latter case is non-dipolar dominated. The results obtained for $f_{\rm mag\_fit}$ also indicate the dependence of the dipolar dominance on the inner core size. The dipolar dominance becomes weaker with a smaller inner core by calculating the dipolar magnetic energy at the CMB (Heimpel *et al.* 2005). In this study, although this tendency was not observed from the dipolarity, it was clear based on the ratio of extrapolation from fitting.

Fig. 11 shows the magnetic energy density at the CMB and surface for two cases; (a) $Ra/Ra_{\rm crit} = 8.0$ at $r_i/r_o = 0.15$ and (b) $Ra/Ra_{\rm crit} = 11.9$ at $r_i/r_o = 0.15$. In case (a), the dipolarity is $f_{\rm dip} = 0.494 > 0.35$ and the ratio of extrapolation from the fitting is $f_{\rm mag\_fit} = 1.435 > 1$. These values mean a dipolar component is dominant. This is consistent with the spectra of the CMB and surface. In case (b), the dipolarity is $f_{\rm dip} = 0.117 < 0.35$ and the ratio of extrapolation from the fitting is $f_{\rm mag\_fit} = 0.322 < 1$. These values mean a dipolar component is not dominant. This is consistent with the spectra of the CMB and surface, which show a quadrupolar component is dominant. The spectra imply that if paleointensity is large, geomagnetic field was not always dipolar-dominated.

Considering both $f_{\rm dip}$ and $f_{\rm mag\_fit}$, Fig. 4 describes the dynamo regime. When the magnetic energy is larger/smaller than the kinetic energy in a simulation case, we categorized this as a strong/weak dynamo. Sustaining the dynamo with a smaller inner core size requires a large Rayleigh number. This is consistent with the findings of Heimpel et al. (2005). At $r_i/r_o = 0.35$, almost all the sustained dynamo cases were strong dipoles. At $r_i/r_o = 0.25$, there were strong dipolar dynamo cases and weak dipolar dynamo cases. At $r_i/r_o = 0.15$, there were weak dipolar and non-dipolar dynamo cases.

In these dynamos, since the Ekman number is $E = 1 \times 10^{-3}$, thermal convection in a rotating spherical shell is not the rapidly rotating regime reported by Gastine et al. (2016) or Long et al. (2020). We calculated the dynamic Elsasser number (Λ_d) defined by Soderlund et al. (2012) in these dynamos to evaluate the relative strength of the Lorentz to Coriolis forces. It is found that Λ_d is approximately 0.01 to 0.1. Therefore, Coriolis force is sufficient to form a columnar convection structure in the dynamos.

The dipolarity at the CMB of the present Earth is $f_{\rm dip} = 0.64$, which is calculated from the 12th IGRF model (Thebault *et al.* 2015). The present radius ratio, r_i/r_o, is 0.35. The range of the dipolarity calculated from results of our numerical simulations of geodynamo for $r_i/r_o = 0.25$ and 0.35 covers the present Earth's dipolarity. The morphology of the sustained magnetic field in both ratios is an Earth-like field. The ratio of the extrapolation from fitting in the present Earth is $f_{\rm mag\_fit} = 4.97$. Here, $f_{\rm mag\_fit}$ is larger than approximately half of the present Earth's value for almost all the cases at $r_i/r_o = 0.35$, while $f_{\rm mag\_fit}$ is smaller than that of almost all the cases at $r_i/r_o = 0.25$. Dipole dominance at $r_i/r_o = 0.35$ is slightly less than that of the present Earth. More magnetic energy, i.e., $l > 2$, is distributed at $r_i/r_o = 0.25$ than the present Earth. In contrast, the dipolarity at $r_i/r_o = 0.15$ is smaller than the present Earth's dipolarity in all cases. The dipole component is not dominant.

In numerical dynamos at $r_i/r_o = 0.35$, we verified that the transition between the dipole and non-dipole is $f_{\rm dip} \approx 0.35$ (Chris-

Table 4. Time average of the kinetic energy $E_{\rm kin}$, magnetic energy $E_{\rm mag}$, dipolarity $f_{\rm dip}$, and Elsasser number Λ for the cases with $r_{\rm i}/r_{\rm o} = 0.35$

$Ra[\times 10^3]$	$Ra/Ra_{\rm crit}$	$E_{\rm kin}$	$E_{\rm mag}$	$f_{\rm dip}$	$f_{\rm mag\_fit}$	$\Lambda_{\rm d}$
84	1.5	35.09	2.376×10^{-3}	–	–	–
110	2.0	43.61	819.6	0.816	4.713	0.420
140	2.5	89.35	1408	0.724	3.174	0.519
170	3.0	106.8	950.2	0.739	4.239	0.407
200	3.6	136.3	890.2	0.692	3.900	0.399
230	4.1	193.1	938.4	0.632	2.946	0.421
280	5.0	311.9	895.6	0.556	2.848	0.383
340	6.1	508.7	713.6	0.480	2.006	0.294
400	7.1	837.6	73.46	0.376	2.071	0.035
450	8.0	1060	10.61	–	–	–

tensen & Aubert, 2006; Olson *et al.* 2011). Our results are consistent with this transition. While dipolarity is an effective index if dynamos can be categorized into large and small dipolarity groups, the combination of dipolarity and the ratio of extrapolation from fitting assesses the dipolar dominance if the dipolarity changes gradually, as in our results.

At $r_i/r_o = 0.15$, an axial dipole formed by a single column (Heimpel *et al.* 2005). In this study, a dipole also formed by some azimuthally localized narrow columns around the dynamo-onset cases. Here, $E_{\rm mag}$ is always smaller than E_{rmkin} in all Ra cases. The magnitude relationship is the same as that of Heimpel et al. (2005). A strong dipole is sustained with a smaller inner core in the fixed flux calculation (Hori *et al.* 2010), changing the core power based on the thermal history (Driscoll 2016), or the buoyancy gained by light elements (@warning Citation '(Lhuillier:2019' on page 6 undefined). Clarifying how heat flow at boundaries sustains the dipole requires further numerical simulations.

Our proposed method of evaluating the dipolar dominance, $f_{\rm mag\_fit}$, enables quantitative investigations of the magnetic field structure in the past environment. Knowledge from paleomagnetic analyses, such as VDM and VGP (virtual geomagnetic pole), is acquired based on the assumption that the geomagnetic field was dipolar-dominated in the past (Merrill *et al.* 1996). In contrast, the VGP paths and actual behavior of the geomagnetic field are not dipolar-dominant. We found that although a dipolar component of magnetic field at the surface is large, the dipolar component is not dominant at the CMB in cases of $Ra/Ra_{\rm crit} > 10.1$ with $r_i/r_o = 0.15$. Our results imply that geomagnetic field could be non-dipolar regardless of strength of paleointensity. Investigation of the numerical dynamo with our proposed method is capable of improving the understanding of the actual behavior of the geomagnetic field and paleomagnetic observations.

5 CONCLUSIONS

As the inner core has been growing for approximately one billion years, sustained dynamo conditions with different inner core sizes are required to understand the past Earth environment. To understand the geometry effect, we performed numerical dynamo simulations with three different radius ratios: $r_i/r_o = 0.15$, 0.25, and 0.35. To evaluate the morphology of the magnetic field, especially the dipole component dominancy, we combined two indices: (i) dipolarity, which is widely used for assessing the relative dipole strength in numerical dynamos, and (ii) the ratio of a dipolar extrapolation from the fitting curve of higher degrees; this method is often used to explain Earth's observed dipolar-dominated field. We verified that the ratio of extrapolation from fitting was valid for determining the dynamo regime. Around the transition between the dipolar and non-dipolar regimes ($f_{\rm dip} \approx 0.35$), we assessed the dipolar dominance using the ratio of extrapolation from fitting. Based on dipolarity and the ratio of extrapolation from fitting, we limited the Ra range of the sustained dynamo for all radius ratios. We found that the Ra range for the strong dipole became narrower with a smaller inner core size. While the dependence of dipolarity on the Rayleigh number is similar at $r_i/r_o = 0.25$ and 0.35, the dipolar dominance becomes weaker with the smaller inner core. There were no strong dipolar dynamos but non-dipolar dynamos at $10.1 < Ra/Ra_{\rm crit} < 15.6$, only at $r_i/r_o = 0.15$. Our results indicate that changes in the radius ratio largely influence the dynamo regime in numerical dynamos with a fixed temperature boundary condition. Further numerical dynamo simulations, by applying different thermal boundary conditions, are required to determine if the intense dipolar magnetic field was sustained in the past Earth with a smaller inner core or entirely without an inner core.

REFERENCES

Al-Shamali, F. M., Heimpel, M. H., & Aurnou, J. M., 2004. Varying the spherical shell geometry in rotating thermal convection, *Geophys. Astrophys. Fluid Dyn.*, **98**(2), 153–169, doi:10.1080/0309192041000165928.

Aubert, J., Labrosse, S., & Poitou, C., 2009, Modelling the paleo-evolution of the geodynamo, *Geophys. J. Int.*, **179**, pp. 1414–1428, doi: 10.1111/j.1365-246X.2009.04361.x.

Biggin, A. J., Piispa, E. J., Pesonen, L. J., Holme, R., Paterson, G. A., Veikkolainen, T., & Tauxe, L., 2015. Palaeomagnetic field intensity variations suggest Mesoproterozoic inner-core nucleation, *Nature*, **526**, pp. 245–248.

Christensen, U. R., Aubert J., Cardin, P., Dormy, E., Gibbon, S., Glatzmaier, G. A., Grote, E., Honkura, Y., Jones, C., Kono, M., Matsushima, M., Sakuraba, A., Takahashi, F., Tilgner, A., Wicht, J. & Zhnag, K., 2001. A numerical dynamo benchmark, *Phys. Earth Planet. Inter.*, **128**, 25–34, doi:10.1016/S0031-9201(01)00275-8.

Christensen, U. R. & Aubert, J., 2006. Scaling properties of convection-driven dynamos in rotating spherical shells and application to planetary magnetic fields, *Geophys. J Int.*, **166**(1), 97–144, doi: 10.1111/j.1365-246X.2006.03009.x

Driscoll, P. E., 2016. Simulating 2 Ga of geodynamo history, *Geophys. Res. Lett.*, **43**, 5680–5687, doi: 10.1002/2016GL068858.

Gastine, T., Wicht, J., & Aubert, J., 2016. Scaling regimes in spherical shell rotating convection, *J. Fluid Mech.*, *808*, 690–732, doi: 10.1017/jfm.2016.659.

Heimpel, M. H., Aurnou, J. M., Al-Shamali, F. M. & Perez N. G., 2005. A numerical study of dynamo action as a function of

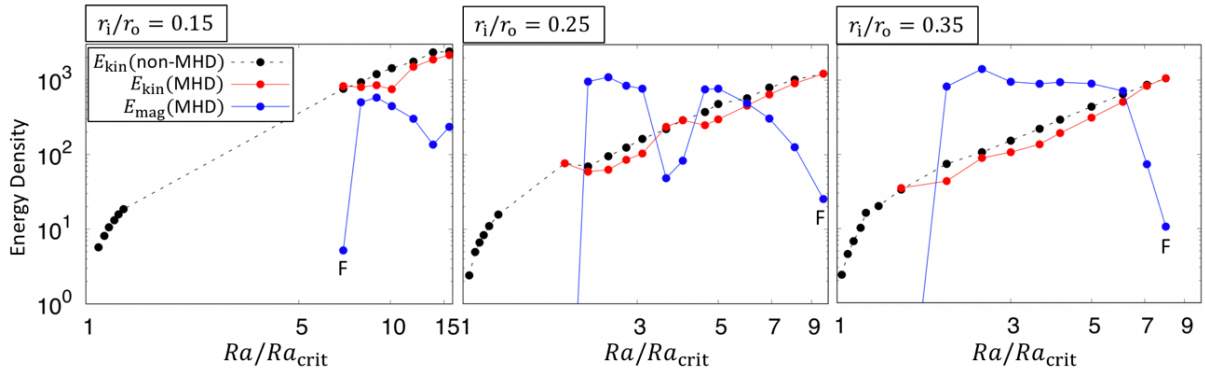

Figure 3. The kinetic and magnetic energy density as a function of the ratio of Rayleigh number to the critical Rayleigh number in spherical shells with different geometries. The black, red, and blue points are the $E_{\rm kin}$ values in the non-MHD cases, $E_{\rm kin}$ values in the MHD cases, and $E_{\rm mag}$ values in the MHD cases, respectively. The "F" denotes the failed dynamo cases.

spherical shell geometry, *Earth planet. Sci. Lett.*, **236**, 542–557, doi:10.1016/j.epsl.2005.04.032.

Hori, K., Wicht, J. & Christensen U. R., 2010. The effect of thermal boundary conditions on dynamo driven by internal heating, *Phys. Earth planet. Inter.*, **182**, 85–97, doi:10.1016/j.pepi.2010.06.011.

Kono, M. & Roberts, P. H., 2002. Recent geodynamo simulations and observations of the geomagnetic field, *Rev. Geophys.*, **40**(4), 1–53, doi: 10.1029/2000RG000102.

Kutzner, C. & Christensen, U. R., 2002. From stable dipolar towards reversing numerical dynamos, *Phys. Earth planet. Inter.*, **131**(1), 29–45, doi: 10.1016/S0031-9201(02)00016-X.

Labrosse, S., Poirier, J.-P., & Le Mouël, J.-L., 2001. The age of the inner core, *Earth Planet. Sci. Lett.*, **190**, 111–123.

Langel, R. A. & Estes, R. H., 1982. A geomagnetic field spectrum, *Geophys. Res. Lett.*, **9**(4), 250–253.

Lhuillier, F., Hulot, G., Gallet, Y. & Schwaiger, T., 2019. Impact of inner-core size on the dipole field behaviour of numerical dynamo simulations, *Geophys. J Int.*, **218**, 179–189, doi: 10.1093/gji/ggz146.

Long, R. S., Mound, J. E., Davis, C. J., & Tobias, S. M., 2020. Scaling behavior in spherical shell rotating convection with fixed-flux thermal boundary conditions, *J. Fluid Mech.*, **889**, doi: 10.1017/jfm.2020.67.

Lowes, F. J., 1974. Spatial power spectrum of the main geomagnetic field, and extrapolation to the core, *Geophys. J Int.*, **36(3)**, 717–730, doi: 10.1111/j.1365-246X.1974.tb00622.x.

Matsui, H., King, E., & Buffett, B., 2014. Multiscale convection in a geodynamo simulation with uniform heat flux along the outer boundary, *Geochem. Geophys. Geosys.*, **15**, 3212–3225, doi:10.1002/2014GC005432.

Merrill, R. T., McElhinny, M. W., & McFadden, P. L., 1996. The Magnetic Field of the Earth: Paleomagnetism, the Core, and the Deep Mantle, Academic Press.

Olson, L. P., Glatzmaier, G. A. & Coe, R. S., 2011. Complex polarity reversals in a geodynamo moidel, *Earth planet. Sci. Lett.*, **304**(1)–(2), 168–179, doi: 10.1016/j.epsl.2011.01.031.

Soderlund, K. M., King, E. M. & Aurnou, J. M., 2012. The influence of magnetic field in planetary dynamo models, *Earth planet. Sci. Lett.*, **333–334**, 9–20, doi: 10.1016/j.epsl.2012.03.038.

Thebault, E., Finlay, C. C., Beggan, C. D., Alken P., Aubert, J., Barrois, O., Bertrand, F., Bondar, T., Boness, A., Brocco, L., Canet, E., Chambodut, A., Chulliat, A., Coisson, P., Civet, F., Du, A., Fournier, A., Fratter, I., Gillet, N., Hamilton, B., Hamoudi, M., Hulot, G., Jager, T., Korte, M., Kuang, W., Lalanne, X., Langlais, B., Leger, J.-M., Lesur V., Lowes, F. J. Macmillan, S., Mandea, M., Manoj, C., Maus, S., Olsen, N., Petrov, V., Ridley, V., Rother, M., Sabaka, T. J., Saturnino, D., Schachtschneider, R., Sirol, O., Tangborn, A., Thomson, A., Toffner-Clausen, L., Vigneron, P., Wardinski, I., & Zvereva, T., 2015. International Geomagnetic Reference Field: the 12th generation, *Earth Planets Space*, **67**:79, doi:10.1186/s40623-015-0228-9.

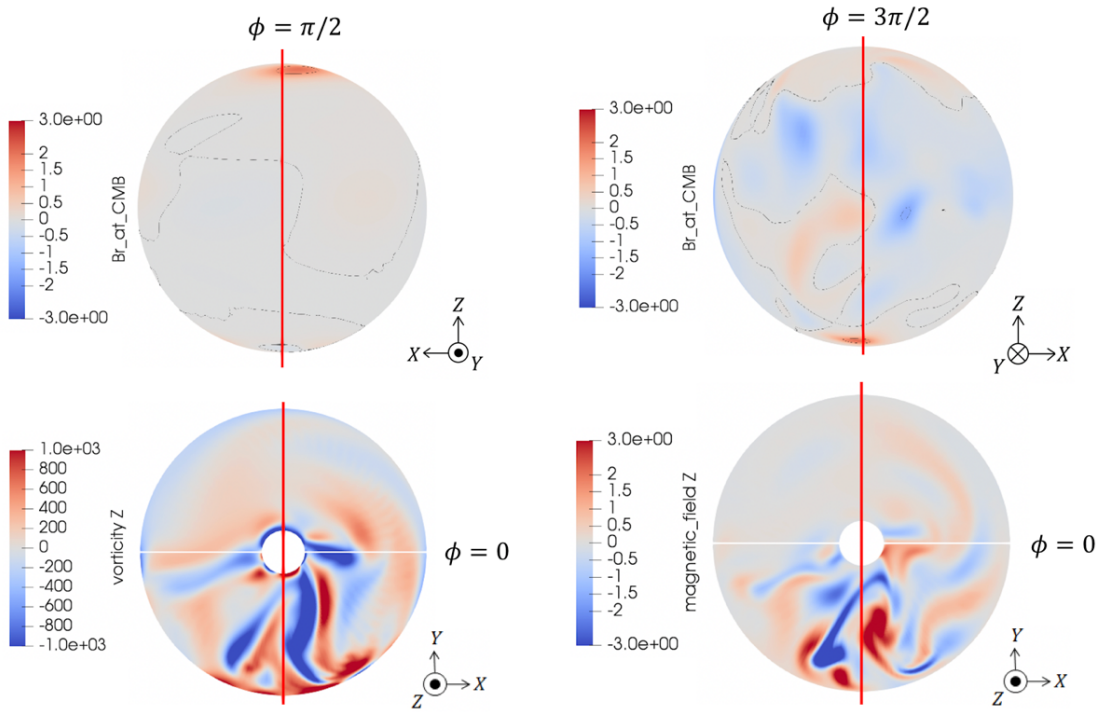

Figure 4. Spatial pattern of the flow and magnetic fields for the case with $Ra/Ra_{\rm crit} = 11.9$ at $r_i/r_o = 0.15$. The radial magnetic field, B_r, at the CMB, viewed from $\phi = \pi/2$ and $3\pi/2$, are plotted in the upper left and right, respectively. The z-component of the vorticity, ω_z, and magnetic field, B_z, at the equatorial plane are plotted in the lower left and right, respectively.

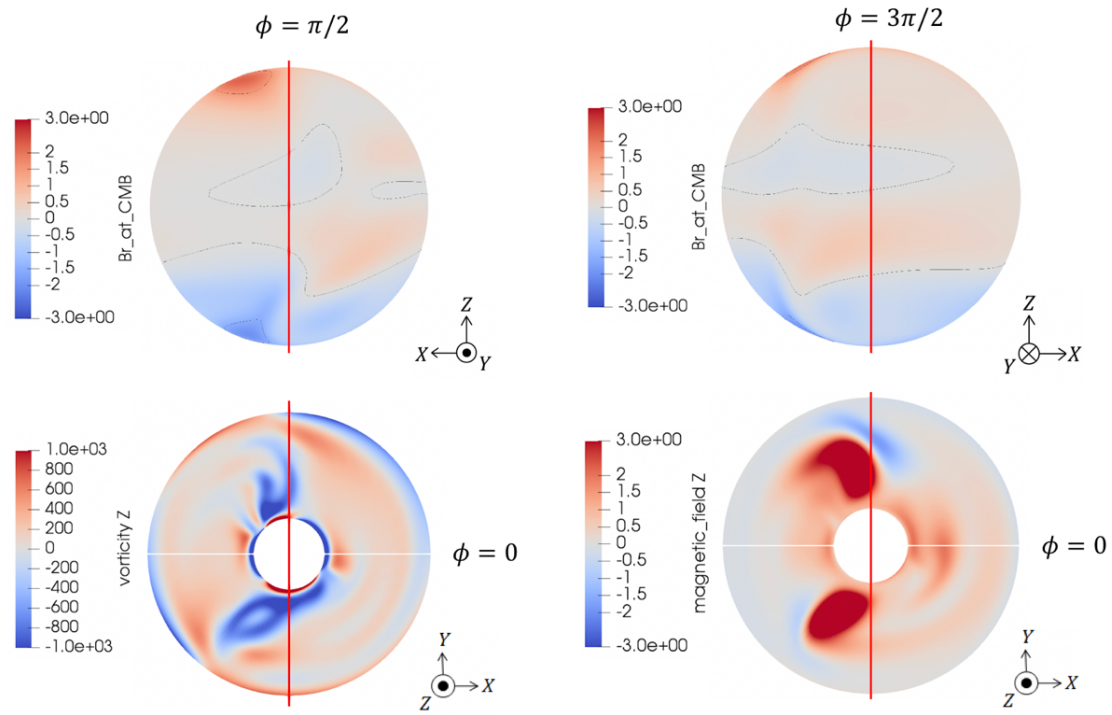

Figure 5. Spatial pattern of the flow and magnetic fields for the case with $Ra/Ra_{\rm crit} = 3.1$ at $r_i/r_o = 0.25$. The radial magnetic field, B_r, at the CMB, viewed from $\phi = \pi/2$ and $3\pi/2$, are plotted in the upper left and right, respectively. The z-component of the vorticity, ω_z, and magnetic field, B_z, at the equatorial plane are plotted in the lower left and right, respectively.

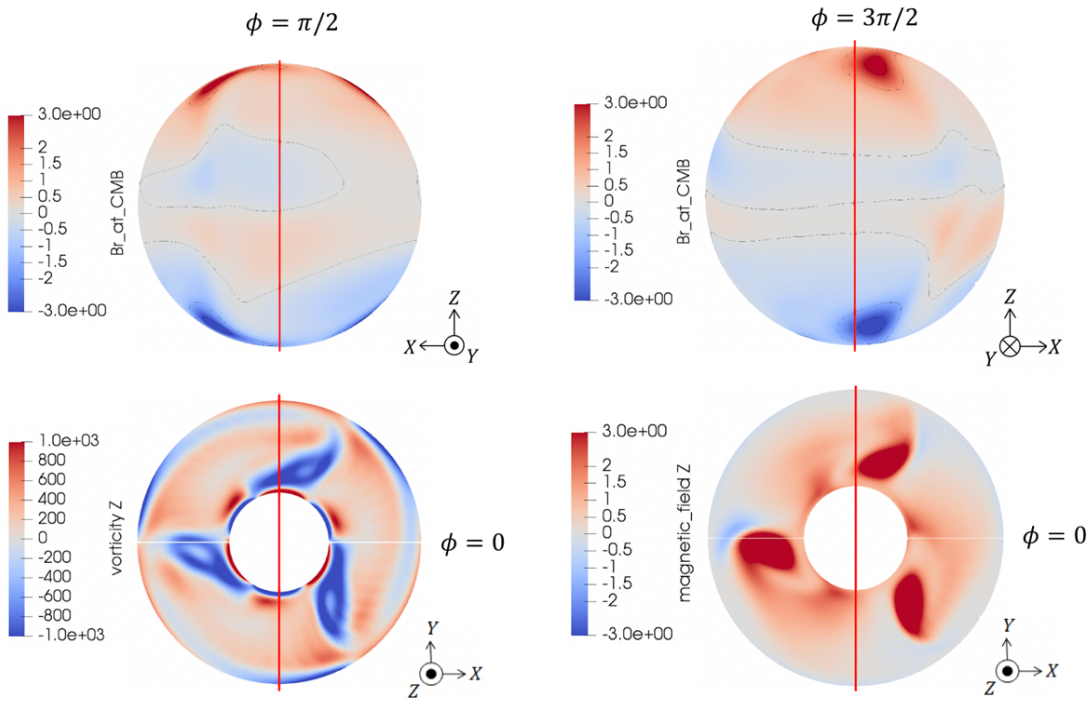

Figure 6. Spatial pattern of the flow and magnetic fields for the case with $Ra/Ra_{\rm crit} = 3.0$ at $r_i/r_o = 0.35$. The radial magnetic field, B_r, at the CMB, viewed from $\phi = \pi/2$ and $3\pi/2$, are plotted in the upper left and right, respectively. The z-component of the vorticity, ω_z, and magnetic field, B_z, at the equatorial plane are plotted in the lower left and right, respectively.

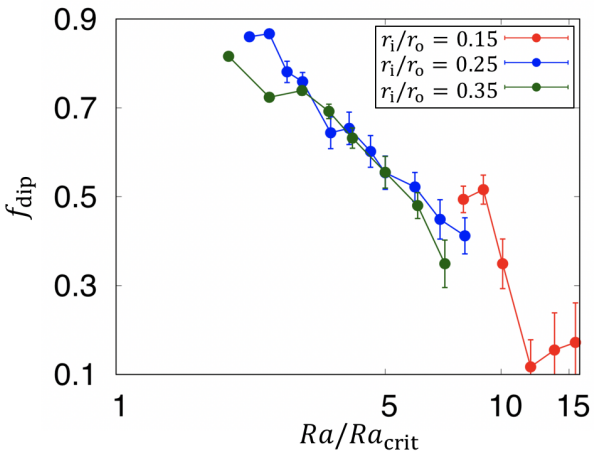

Figure 7. Dipolarity $f_{\rm dip}$ as a function of the ratio of Rayleigh number to the Critical Rayleigh number for different spherical shell geometries. The red, blue, and green points indicate the cases of $r_i/r_o = 0.15$, 0,25, and 0.35, respectively. The bar represents the standard deviation.

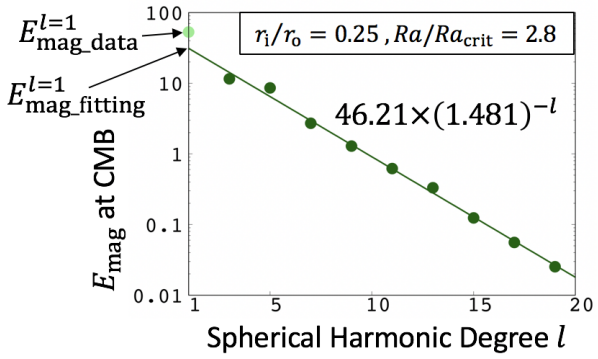

Figure 8. Magnetic energy density at the CMB of simulation data in the spherical harmonics degree $l = 1$ and fitting value of $l = 1$ as a function of spherical harmonic degree for $r_i/r_o = 0.25$ and $Ra/Ra_{\rm crit} = 2.8$.

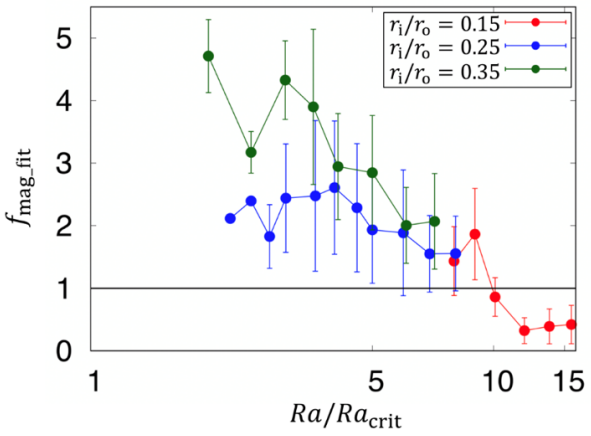

Figure 9. The ratio of the dipolar magnetic energy density at the CMB to the extrapolation of the spherical harmonic degree $l = 1$, $f_{\mathrm{mag\_fit}}$, as a function of the ratio of Rayleigh number to the critical Rayleigh number for different geometries. The red, blue, and green points indicate the cases of $r_i/r_o = 0.15$, 0,25, and 0.35, respectively. The bar represents the standard deviation.

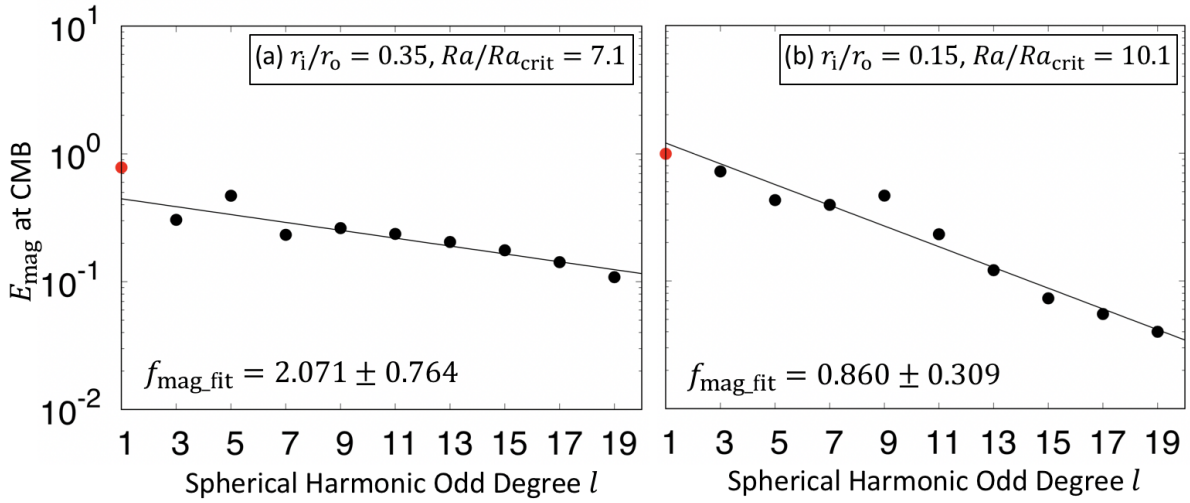

Figure 10. Magnetic energy density at the CMB of simulation data at $l = 1$ and fitting value of $l = 1$ as a function of spherical harmonic odd degrees. (a) Dipolar case at $Ra/Ra_{\mathrm{crit}} = 7.1$ at $r_i/r_o = 0.35$, and (b) Non-dipolar case at $Ra/Ra_{\mathrm{crit}} = 10.1$ at $r_i/r_o = 0.15$.

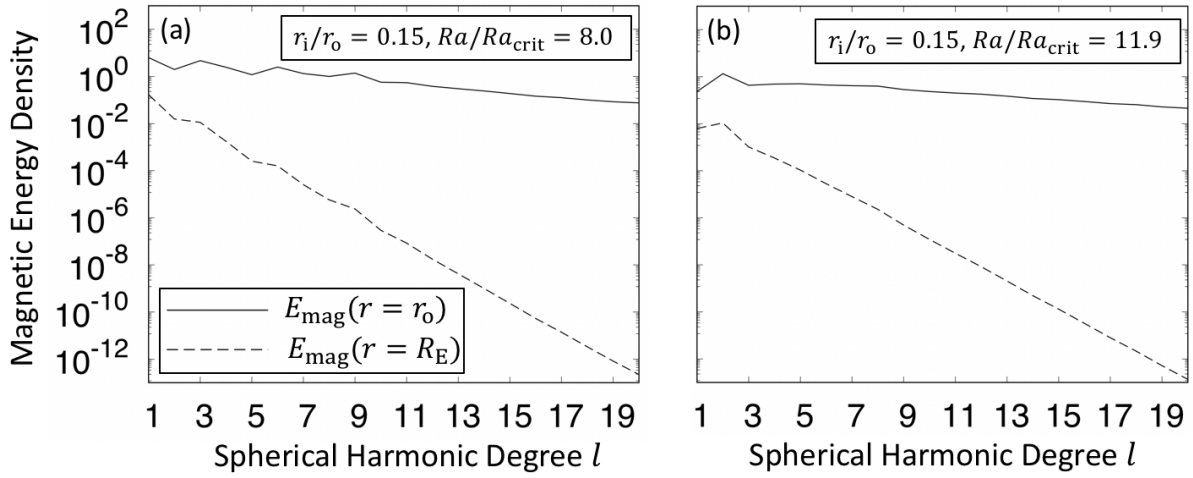

Figure 11. Magnetic energy density at the CMB and surface of simulation data as a function of spherical harmonic degree. (a) Dipolar case at $Ra/Ra_{\mathrm{crit}} = 8.0$ at $r_i/r_o = 0.15$, and (b) Non-dipolar case at $Ra/Ra_{\mathrm{crit}} = 11.9$ at $r_i/r_o = 0.15$.

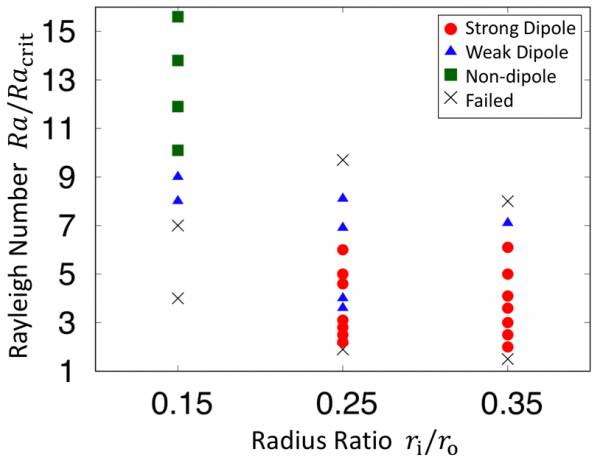

Figure 12. Dynamo regime in $r_i/r_o = 0.15$, 0.25, and 0.35. Red circles, blue triangles, green squares, and black crosses represent strong dipolar, weak dipolar, non-dipolar, and failed dynamo cases, respectively.